ЯДЕРНА ФІЗИКА
NUCLEAR PHYSICS

УДК 539.142 https://doi.org/10.15407/jnpae2024.03.228

A. A. Alzubadi*, S. M. Aldulaimi

Department of Physics, College of Science, University of Baghdad, Baghdad, Iraq

*Corresponding author: ali.abdullatif@sc.uobaghdad.edu.iq

RELATIVISTIC MEAN FIELD ANALYSIS OF TRIAXIAL DEFORMATION FOR NUCLEI NEAR THE NEUTRON DRIP LINE

The present study focuses on the deformation of neutron-rich nuclei near the neutron drip line. The nuclei of interest include ^{28}O, ^{42}Si, ^{58}Ca, ^{80}Ni, ^{100}Kr, ^{122}Ru, ^{152}Ba, ^{166}Sm, and ^{176}Er. The relativistic Hartree - Bogoliubov (RHB) approach with effective density-dependent point coupling is utilized to investigate the triaxial deformation, and Skyrme - Hartree - Fock + Bardeen - Cooper - Schrieffer is used to analyze the axial deformation. The study aimed to understand the interplay between nuclear forces, particle interactions, and shell structure to gain insights into the unique behavior of neutron-rich nuclei. Despite these nuclei containing magic numbers, their shapes are still affected by the nucleons' collective behavior and energy levels. As the number of neutrons increases, the shape smoothly transitions from spherical to triaxial and then to prolate. The axial deformation analysis confirmed the results of the triaxial deformation analysis using the RHB method. An imbalance in the number of protons and neutrons can affect pairing energy, where extra neutrons can reduce overall pairing energy, and protons can disrupt the nucleon pairing due to stronger Coulomb repulsion between them.

Keywords: relativistic mean-field, Hartree - Fock + Bardeen - Cooper - Schrieffer, triaxial deformation, neutron dripline, collective motion.

1. Introduction

The nuclear shape can deviate from its spherical shape, it undergoes deformation. This deformation can be triggered by factors like the shell structure, the presence of high spin states, and the collective motions. In deformed nuclei, shape transition occurs from spherical to axial or triaxial shape. The axial deformation is an indication of whether the shape is oblate or prolate, while in a triaxial deformation, the nucleus has three axes of symmetry, each with varying lengths. This leads to intriguing effects such as alterations in energy levels, increased stability, and changes in decay rates. Basically, triaxial deformation of nuclei can be achieved in two ways. Firstly, through motion, where groups of nucleons move together in a manner resulting in a deformed nucleus. Secondly, the presence of a band occurs when a nucleus rapidly rotates around its axis, causing elongation and distortion [1].

It is well-known that studying the triaxial deformation of nuclei provides insights into nuclear structure, particularly energy levels, decay rates, and nuclear reactions. These findings hold potential for applications in the nuclear energy and medical fields. Various theoretical models can be used to investigate the triaxial shape of nuclei, each with its own set of advantages and disadvantages. For instance, the Nilsson model, Interacting Boson Model, Hartree - Fock - Bogoliubov (HFB) model, and Relativistic Mean Field (RMF) model [2]. The present work will utilize the RMF model to analyze the triaxial quadrupole shapes of nuclei near the neutron dripline, encompassing a wide range in the nuclear chart. In this model, protons and neutrons are considered fundamental particles that interact with each other through the exchange of scalar (σ) and vector (ω) mesons. These mesons represent the attractive and repulsive components of the nuclear interaction, respectively [3]. To accurately analyze the influence of triaxial deformation, it is necessary to expand the potential with axial symmetry using Legendre polynomials up to high orders. This expansion permits non-zero values for quadrupole, octupole, and hexadecapole moments, which characterize the triaxial shape of the nucleus. Using RMF, extensive theoretical studies were conducted to analyze the nuclear structure.

Koepe and Ring [4] investigated the ground state shape of the ^{24}Mg nucleus within the framework of a constrained three-dimensional RMF, particularly the energy surface as a function of the quadrupole deformation parameters β_2 and γ. Lalazissis and Sharma [5] studied the ground-state properties of some exotic nuclei near the $Z = 40$ region using RMF. They also anticipated the presence of shape coexistence in heavy isotopes. Hirata et al. [6] studied the triaxial deformation of some light-unstable nuclei using RMF. Yao et al. [7] extended the RMF by including time-odd fields and used it to study the candidate multiple chiral doublets nuclei. Yao et al. [8, 9] also developed a structure model that employs the generator coordinate approach to blend angular-momentum projected wave functions produced by constrained self-consistent RMF calculations for triaxial

shapes. Lu et al. [10] developed the multidimensionally-constrained RMF to study the effect of triaxiality in some even-even actinide nuclei. Xue et al. [11] studied the hyperon impurity effect on the low-lying states of *sd*-shell nuclei based on RMF. Abusara et al. [12] calculated the triaxiality softness and shape coexistence in Mo and Ru isotopes using the relativistic Hartree - Bogoliubov (RHB) model. Nabi et al. [13] investigated the nuclear structure properties of $N = 50$ and 82 isotones using the RMF model. Kumar et al. [14] investigated the shape evolution of the isotopic chains of shell closure $Z = 8$, 20, 28, and 50 using RHB. Recently, Rong et al. [15] investigated the triaxial and octupole shapes in ^{96}Zr by employing the RHB model.

In the present work, we explore the presence of triaxial deformation in light, medium, and heavy nuclei located near the neutron driplines using the RHB model. In particular, ^{28}O, ^{42}Si, ^{58}Ca, ^{80}Ni, ^{100}Kr, ^{122}Ru, ^{152}Ba, ^{166}Sm, and ^{176}Er nuclei, give insight into the evolution of nuclear deformation in the neutron-rich even-even nuclei. The evolution of nuclear deformation is closely related to shell evolution, as changes in deformation can be correlated with the rearrangement of nucleons in the nuclear energy levels. Additionally, the collective excitations include rotational and vibrational modes and nuclear stability. For comparison with non-relativistic nuclear models, which rely on axially symmetric deformation, we have implemented the Skyrme - Hartree - Fock (SHF) + Bardeen - Cooper - Schrieffer (BCS) calculations for studying the deformation-energy surfaces for the selected neutron-rich nuclei.

The current research will be organized in the following manner: Section 2 will provide a concise overview of the theoretical formalism of the RHB model employed in the present analysis. Section 3 will present and analyze the calculated results. Lastly, Section 4 will summarize the results and conclusions drawn from the analysis.

2. Nuclear deformation

The excitation spectra of even-even nuclei up to approximately 2 MeV are usually explained as rotations and vibrations of the nucleus. According to the collective model framework, an even-even nucleus is considered a homogeneous nuclear matter – a quantum droplet of deformable matter. Unsurprisingly, the greater the number of nucleons in the nucleus, the more significant the collective effects are in that nucleus.

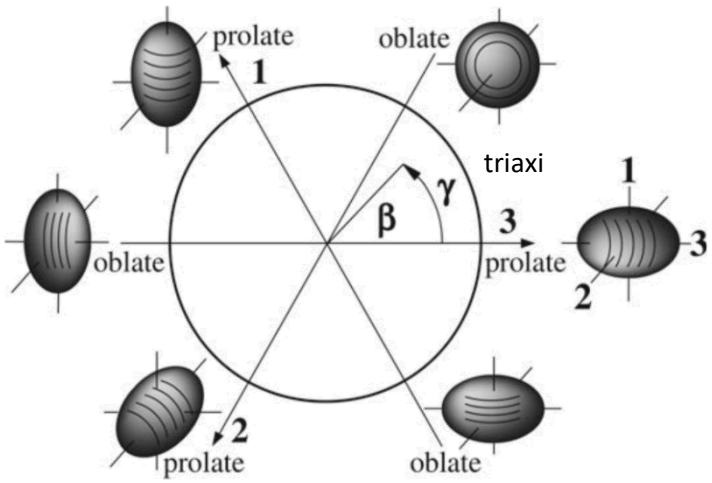

Fig. 1. The relationship between the deformation parameters β, γ, and the nuclear shape.

Based on the details shown in Fig. 1, it is possible to depict nuclear quadrupole deformation using symmetry arguments. The value of γ ranges from 0º, which represents a strictly prolate shape, to 60º, which represents a purely oblate shape. Any angle between 0 and 60º indicates a triaxial nucleus, which lacks a distinct axis of symmetry [2]. These sextants are generally referred to as potential energy surfaces (PES).

3. Theoretical framework

There is a specific category of self-consistent mean-field (SCMF) structure models that rely on relativistic (covariant) energy density functionals. These models have proven to be effective in examining various nuclear structure phenomena, and their accuracy is comparable to the non-relativistic HFB approach that uses Skyrme functionals or Gogny effective interactions. As previously stated, this section will provide a brief overview of the RHB model as it is currently implemented in RMF. Covariant density functional theory employs various models to depict the nucleus. The present work uses the density-dependent point-coupling (DD-PC1) model to perform our calculations. The mesons are absent in this model and thus use a zero-range interaction. It provides an excellent description of different ground and excited states over the entire nuclear chart. The details of each model are discussed below.

3.1. Lagrangian density for the point coupling models

The point-coupling models provide an alternative method for conveying the self-consistent relativistic mean-field framework [16]. In this model, the isoscalar-scalar σ meson, the isoscalar-vector ω meson, and the isovector-vector ρ meson build the minimal set of meson fields necessary for quantitatively describing nuclei. An effective Lagrangian that includes the isoscalar-scalar, isoscalar-vector, and isovector-vector four-fermion interactions is given by the following equation [17, 18]:

$$\mathcal{L} = \bar{\psi}\left(i\gamma\cdot\partial - m\right)\psi - \frac{1}{2}\alpha_S\left(\hat{\rho}\right)\left(\bar{\psi}\psi\right)\left(\bar{\psi}\psi\right) -$$

$$-\frac{1}{2}\alpha_V\left(\hat{\rho}\right)\left(\bar{\psi}\gamma^{\mu}\psi\right)\left(\bar{\psi}\gamma_{\mu}\psi\right) -$$

$$-\frac{1}{2}\alpha_{TV}\left(\hat{\rho}\right)\left(\bar{\psi}\vec{\tau}\gamma^{\mu}\psi\right)\left(\bar{\psi}\vec{\tau}\gamma_{\mu}\psi\right) -$$

$$-\frac{1}{2}\delta_S\left(\partial_{\nu}\bar{\psi}\psi\right)\left(\partial^{\nu}\bar{\psi}\psi\right) - e\bar{\psi}\gamma\cdot A\frac{1-\tau_3}{2}\psi, \quad (1)$$

where m is the nucleon's mass and ψ denotes the Dirac spinor. The four-fermion coupling constants are stated by α_s, α_v, and α_{tv}. The model contains the coupling of protons to the electromagnetic field along with the free-nucleon Lagrangian and point-coupling interaction terms, which are given by the following equations respectively [16]:

$$L_m = \bar{\psi}\left(i\gamma_{\mu}\partial^{\mu} - m\right)\psi, \quad (2)$$

$$L_m = \frac{1}{2}\partial_{\mu}\sigma\partial^{\mu}\sigma - \frac{1}{2}m_{\sigma}^2\sigma^2 - \frac{1}{2}\Omega_{\mu\upsilon}\Omega^{\mu\upsilon} +$$

$$+\frac{1}{2}m_{\omega}^2\omega_{\mu}\omega^{\mu} - \frac{1}{4}\vec{R}_{\mu\upsilon}.\vec{R}^{\mu\upsilon} + \frac{1}{2}m_{\rho}^2\vec{\rho}_{\mu}.\vec{\rho}^{\mu} - \frac{1}{4}F_{\mu\upsilon}F^{\mu\upsilon} \quad (3)$$

with the corresponding masses m_σ, m_ω, m_ρ, and $\Omega_{\mu\nu}$, $R_{\mu\nu}$, $F^{\mu\nu}$ are field tensors field tensors

$$\Omega_{\mu\upsilon} = \partial_{\mu}\omega_{\nu} - \partial_{\nu}\omega_{\mu}, \quad (4)$$

$$\vec{R}_{\mu\upsilon} = \partial_{\mu}\vec{\rho}_{\upsilon} - \partial_{\upsilon}\vec{\rho}_{\mu}, \quad (5)$$

$$F_{\mu\upsilon} = \partial_{\mu}A_{\upsilon} - \partial_{\upsilon}A_{\mu}. \quad (6)$$

The derivative terms in Eq. (1) take into account the leading effects of finite-range interactions, which are essential for a quantitative representation of the nuclear characteristics. The chosen point couplings' functional form is

$$\alpha_i\left(\rho\right) = a_i + \left(b_i + c_i\,x\right)e^{-d_i x}, \ \left(i = S, V, TV\right) \quad (8)$$

where $x = \rho/\rho_{sat}$, and ρ_{sat} represents the density of nucleons in symmetric nuclear matter at saturation. For the current analysis, we will utilize the triaxial RHB [16, 19], which features a separable pairing model. The calculations with constraints are carried out by applying restrictions on the axial and triaxial mass quadrupole moments. The PES analysis, which involves studying the quadrupole deformation parameter, is conducted using the quadratic-constrained method [20]. The quadratic constraint approach makes use of an unrestricted variant of the function denoted by:

$$\left\langle\hat{H}\right\rangle + \sum_{\mu=0,2} C_{2\mu}\left(\left\langle\hat{Q}_{2\mu}\right\rangle - q_{2\mu}\right)^2, \quad (8)$$

where $\hat{H}$ represents the total energy, and $\hat{Q}_{2\mu}$ is the expectation value of the mass quadrupole operators

$$\hat{Q}_{20} = 2Z^2 - X^2 - Y^2 \text{ and } \hat{Q}_{22} = X^2 - Y^2 \quad (9)$$

$q_{2\mu}$ is the constrained value of the multipole moment, and $C_{2\mu}$ is the corresponding stiffness constant [20]. To achieve a self-consistent solution, the quadratic constraint introduces an additional force term $\sum_{\mu=0,2}\lambda_{\mu}\hat{Q}_{2\mu}$ to the system, where $\lambda_{\mu} = 2C_{2\mu}\left(\hat{Q}_{2\mu} - q_{2\mu}\right)$. Such a term is necessary to force the system to a point different from the stationary point in deformation space. In general, the self-consistent solution and constrained values $q_{2\mu}$ coincide only at the stationary point for the quadrupole moments $\langle Q_{2\mu}\rangle$. The augmented Lagrangian [21] method has been implemented to resolve the convergence problem of the self-consistent procedure that diverges when the stiffness constant $C_{2\mu}$ is increased. These operators are related to the axially-symmetric deformation β and triaxiality γ as follows [22]

$$\beta = \sqrt{\frac{5}{16\pi}}\frac{4\pi}{3}\frac{1}{A\left(r_0A^{1/3}\right)^2}\sqrt{\hat{Q}_{20}{}^2 + 2\hat{Q}_{22}{}^2}, \quad (10)$$

$$\gamma = \arctan\sqrt{2}\frac{\hat{Q}_{22}}{\hat{Q}_{20}}, \quad (11)$$

3.2. SHF + BCS calculations

The SCMF based on SHF plus BCS calculations is designed to describe the structure of nuclei and study the shape evolution and transitional in nuclear density shapes, where the pairing correlation has been considered. SHF is the best method for anticipating closed-shell nuclei's total binding and single-particle energies [22]. Also, it is a valuable tool because this force is central and has zero-range interactions [23].

The building block of a mean-field theory is a set of single-particle wave functions ψ_α together with fractional occupation amplitudes υ_α, i.e., [24]

$$\{\psi_\alpha, \upsilon_\alpha, \alpha = 1, ..., \Omega\}, \quad (12)$$

where Ω denotes the size of the active single-particle space and occupation amplitudes are limits to the interval $0 \le \upsilon_\alpha \le 1$. The complementary non-occupation amplitude is $u_\alpha = \sqrt{1-\upsilon_\alpha^2}$.

The BCS many-body state composed of these ingredients is

$$|\phi\rangle = \prod_{\alpha>0}\left(u_\alpha + \upsilon_\alpha \alpha_\alpha^+ \alpha_{\bar{\alpha}}^+\right)|0\rangle, \quad (13)$$

where $|0\rangle$ is the particle-vacuum state, α_α^+ the creation operator for a Fermion in state ψ_α, and $\bar{\alpha}$ the time-reversed partner to state α. The local nucleon density is defined as [24]

$$\rho_q(\vec{r}) = \sum_{\alpha\in q}\sum_s \upsilon_\alpha^2 \left|\psi_\alpha(\vec{r}, s)\right|^2. \quad (14)$$

The total energy is composed as

$$E_{tot} = T + E_{Skyrme} + E_{Coulomb} + E_{pair} + E_{cm}, \quad (15)$$

where E_{Skyrme} is the Skyrme energy, and $E_{Coulomb}$ is the Coulomb energy

$$E_C = \frac{e^2}{2}\int dV dV' \frac{\rho_p(\vec{r})\rho_p(\vec{r}')}{|\vec{r}-\vec{r}'|} - \int dV \frac{3e^2}{4}\left(\frac{3}{\pi}\right)^{\frac{1}{3}}\rho_p^{4/3} \quad (16)$$

and the pairing energy is

$$E_{pair} = \frac{1}{4}\sum_{q\in\{p,n\}} V_{pair,q}\int dV \left|\xi_q\right|^2\left[1 - \frac{\rho}{\rho_{0,pair}}\right], \quad (17)$$

where dV stands for the volume element in full three-dimensional space, e is the elementary charge with e^2 = 1.43989 MeV/c·fm, and ξ_q is the pairing density

$$\xi_q(\vec{r}) = \sum_{\alpha\in q}\sum_s w_\alpha u_\alpha \upsilon_\alpha \psi_{\bar{\alpha}}(\vec{r}, s)\psi_\alpha(\vec{r}, s), \quad (18)$$

where w_α stands for a soft cut-off of pairing space. The $s \in \pm 1$ variables indicate the spinor component of the wave functions. The pairing energy contains the parameter $\rho_{0,pair}$ that regulates the balance between volume and surface pairing. Nuclear deformation is defined as the deviation from the spherical symmetry about the center of mass (c.m.) which is expressed by the electric quadrupole moment. Thus, the most important moments are the center of mass moments

$$\vec{R}_{type} = \frac{\int dV \vec{r}\rho_{type}(\vec{r})}{\int dV \rho_{type}(\vec{r})}, \quad (19)$$

where "'type" can refer to proton from ρ_p neutron from ρ_n isoscalar or total from the total density $\rho = \rho_p + \rho_n$, or isovector moment from the isovector density $\rho_T = 1 = (N/A)\rho_p - (Z/A)\rho_n$.

The anisotropic combinations can be quantified in terms of the spherical quadrupole moments

$$Q_{2m,type} = \int dV r^2 Y_{2m}\rho_{type}\left(\vec{r} - \vec{R}_{type}\right). \quad (20)$$

The axial symmetry allows non-vanishing quadrupole moments only for m = 0. It is often convenient to express them as a dimensionless quadrupole moment (quadrupole deformation parameter)

$$\beta_{20} = \frac{4\pi}{3}\frac{Q_{20}}{AR^2}. \quad (21)$$

All wavefunctions and fields are defined on an axial coordinate-space grid. The axial coordinates and their relation to Cartesian coordinates are

$$r = \sqrt{x^2 + y^2}, \quad z = z, \quad (22)$$

where r stands for the axial coordinate expressing the distance of the space point to the symmetry axis. Axially symmetric objects, like densities and potentials, depend only on the r and z. r and z are both represented on an equidistant grid:

$$r \leftrightarrow \{r_0, ..., r_{N_r}\}, \quad r_\upsilon = \upsilon\,\Delta r, \quad (23)$$

$$z \leftrightarrow \{(z_{-N_z} ... z_{-1}), z_0, ..., z_{N_z}\}, z_\upsilon = \upsilon\,\Delta z, \quad (24)$$

where Δr and Δz are numerical parameters for the grid spacing. Along the z-axis, the filled grid from $-N_z$ to $+N_z$ allows reflection-asymmetric nuclear configurations or from 0 for $+N_z$ plus exploiting reflection symmetry to reconstruct the whole grid. Densities and potentials are axially symmetric functions $f(r, z)$ and trivially represented as $f(r_{\upsilon r}, z_{\upsilon z})$ on the grid. A single-particle wavefunction has a richer structure with angular dependence and spin. It is represented as [24]

$$\psi_\alpha = \begin{pmatrix} \psi_\alpha^{(+)}\left(r_{\upsilon_r}, z_{\upsilon_z}\right)\exp\left(i m_\alpha \phi\right) \\ \psi_\alpha^{(-)}\left(r_{\upsilon_r}, z_{\upsilon_z}\right)\exp\left(i\left(m_\alpha + 1\right)\phi\right) \end{pmatrix}, \quad (25)$$

where m_α is the z-component of orbital angular momentum of the upper spin component with $k_\alpha = m_\alpha + 1/2$ being then the z-component of total z angular momentum.

In the previous section, we gave an overview of the formalisms used. Further details can be found in the References.

4. Results and discussions

In our current investigation, we have conducted a thorough analysis of the axial and triaxial nuclear deformation for a set of neutron-dripline nuclei including ^{28}O, ^{42}Si, ^{58}Ca, ^{80}Ni, ^{100}Kr, ^{122}Ru, ^{152}Ba, ^{166}Sm, and ^{176}Er. The results obtained from the triaxially deformed RMF model provide an essential insight into our research and play a crucial role as one of the fundamental degrees of freedom. Its significance is evident in various phenomena such as nuclear fission, nuclear chirality, and wobbling motion. As previously mentioned, triaxial deformation can be characterized by the asymmetry of the nucleus in three different directions, giving rise to complex nuclear behaviors. Fig. 2 presents self-consistent RHB triaxial quadrupole binding-energy maps of the selected dripline nuclei in the β-γ plane using DD-PC1 parameterization. The step size for β_2 is 0.05 and 5º for γ. It is clear that when γ equals 0º, the structure is axial prolate, while at 60º, it becomes oblate. The $0^o < \gamma < 60^o$ values give us the triaxial shapes.

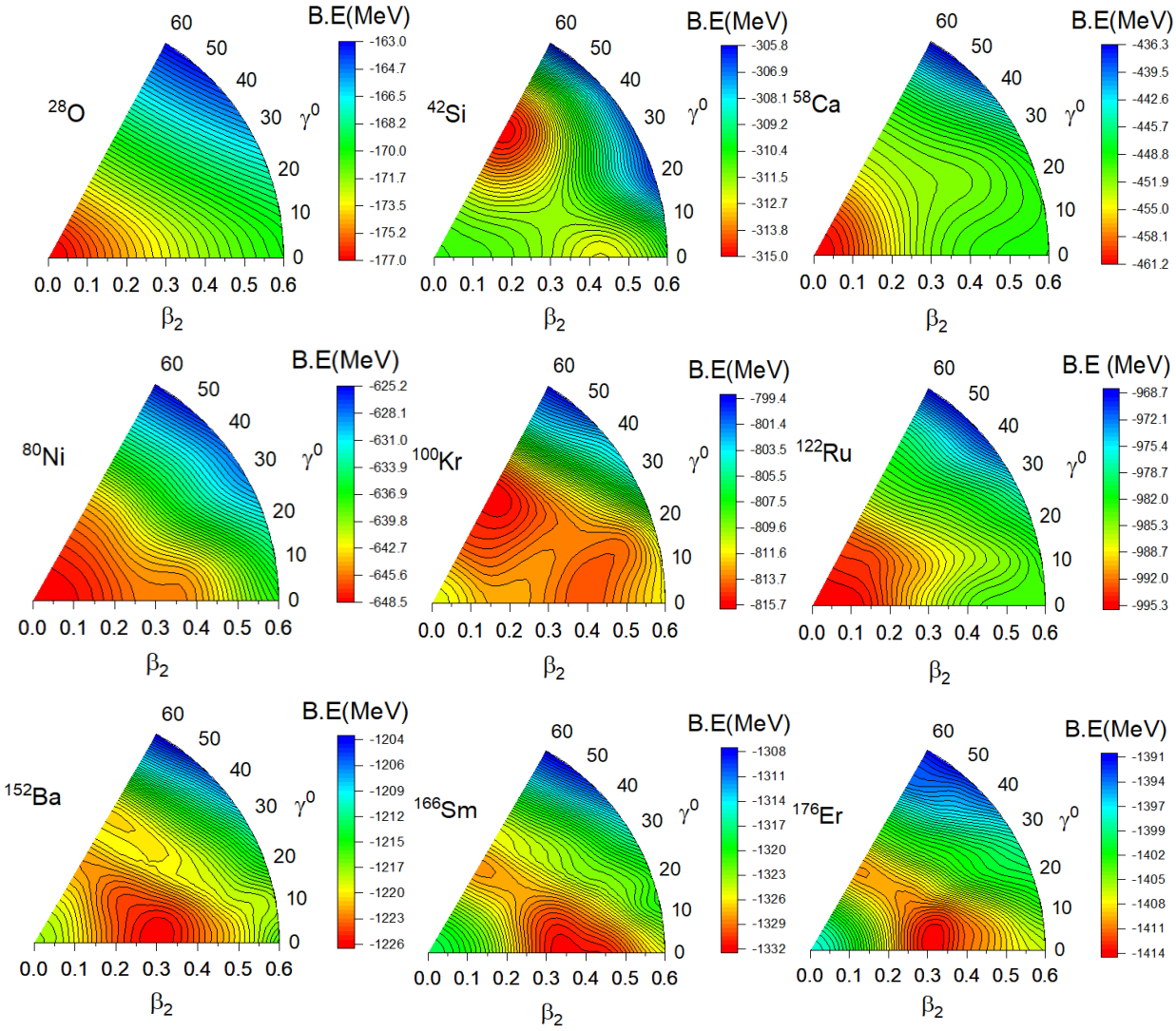

Fig. 2. The triaxial quadrupole energy surfaces obtained using the triaxially deformed RMF calculations for ^{28}O, ^{42}Si, ^{58}Ca, ^{80}Ni ^{100}K, ^{122}Ru, ^{152}Ba, ^{166}Sm, and ^{176}Er neutron-rich nuclei in the β-γ plane $(0^\circ \le \gamma \le 60^\circ)$. (See color Figure on the journal website.)

The energy maps depicted in Fig. 2 vividly illustrate the triaxial deformation of dripline nuclei. The maps demonstrate the gradual transition from spherical neutron closed-shell nuclei to oblate and shape coexistence and finally to strongly prolate deformed nuclei. By analyzing our results depicted in Figs. 2 and 3, we can explain the shape of each nucleus based on its axial and triaxial deformations. The current calculations for axial deformation were compared with HFB calculations using the Gogny interaction [25].

The comparison showed a strong correspondence with the overall trends observed in this study. Additionally, they were also compared in the Table with the ground state deformation values of Moller et al. [26], which are based on the finite-range droplet macroscopic model and the folded-Yukawa single-particle microscopic model. Examining these values shows a good agreement with the data from Moller et al.

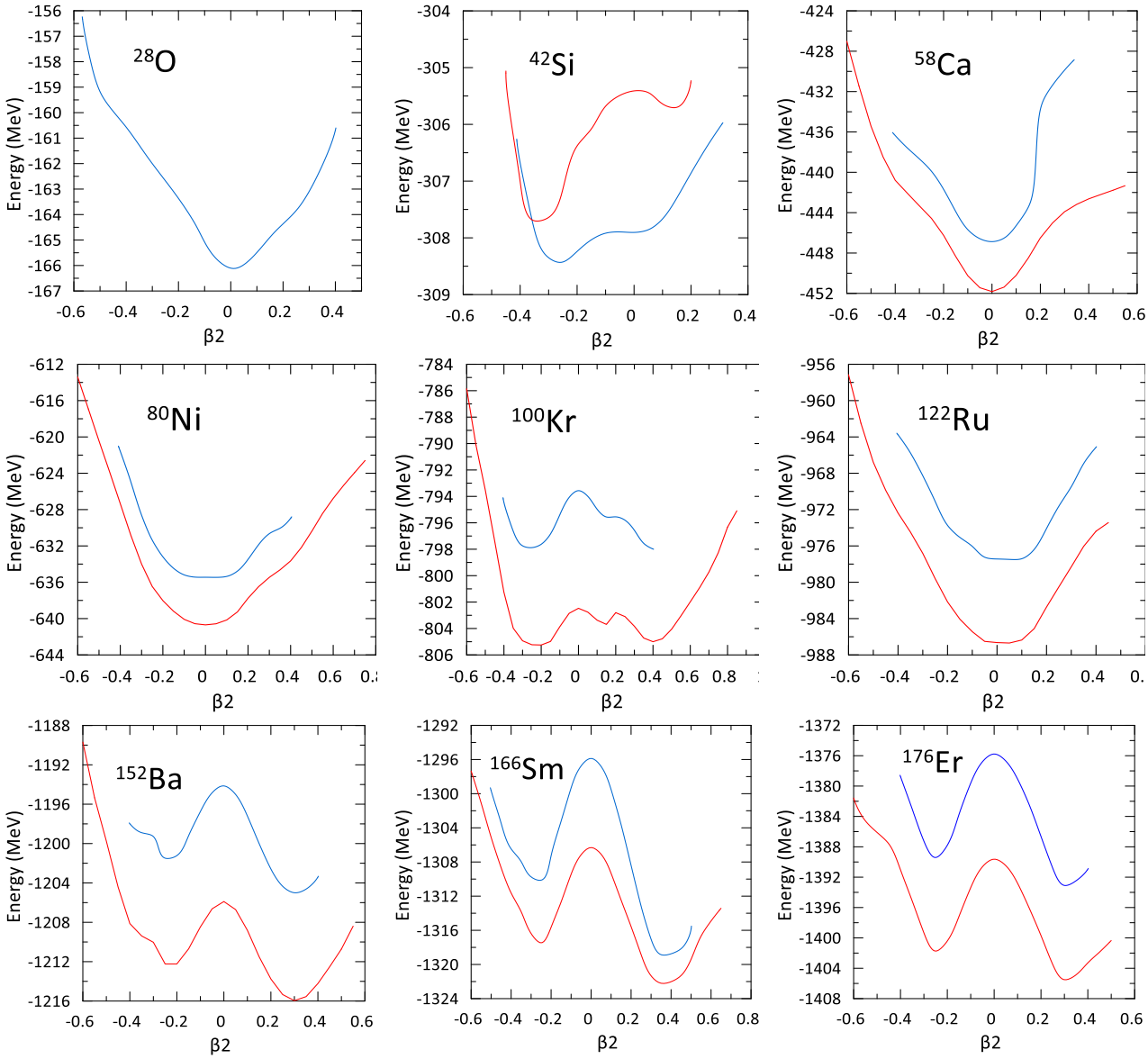

Fig. 3. The calculated PES as a function of quadrupole deformation parameter β_2 obtained using HF + BCS axial calculation with Skyrme interaction (*blue line*) for ^{28}O, ^{42}Si, ^{58}Ca, ^{80}Ni ^{100}K, ^{122}Ru, ^{152}Ba, ^{166}Sm, and ^{176}Er neutron-rich nuclei in comparison with HFB calculations with Gogny interaction. The contours join points on the surface with the same energy. (See color Figure on the journal website.)

Comparison of current β_2 and BE with those from Moller et al. [26]

Nucleus	β_2 equilibrium present work	β_2 equilibrium [26]	BE, MeV present work	BE, MeV [26]
^{28}O	0.012	0.000	166.118	166.82
^{42}Si	−0.309	−0.313	308.3100	313.99
^{58}Ca	0.000	0.001	446.8711	453.450
^{80}Ni	0.000	0.000	635.4481	647.38
^{100}Kr	−0.303	0.342	797.7160	815.19
^{122}Ru	−0.151	−0.124	975.0439	993.28
^{152}Ba	0.252	0.249	1204.383	1225.37
^{166}Sm	0.301	0.297	1309.852	1332.43
^{176}Er	0.251	0.278	1390.8757	1414.69

Upon inspection of the contour plots, it is evident that the nucleus ^{28}O has a spherical shape, with β and γ equal to 0. This behavior is also emphasized in the axial symmetric potential energy curve in Fig. 3. The nuclear shape of ^{42}Si is different from ^{28}O. This nucleus has a magic number, $N = 28$, that requires a strong spin-orbit interaction [27]. The ground state is localized around the oblately deformed energy minimum at (β, γ) = (0.35, 60º). Although there is no local minimum at the spherical shape, the energy of the spherical state is relatively lower than the deformed states, and the shell gap was observed to disappear gradually. According to the triaxial and axial PESs shown in Figs. 2 and 3, it can be inferred that ^{58}Ca and ^{80}Ni nuclei, which have a single-shell closure, exhibit a spherical shape with values of β = γ = 0. The contour plot for the PES of ^{100}Kr nucleus interestingly shows a sharp transition from a prolate ground state to an oblate one. The occurrence of a triaxial shape transition can be attributed to the competition between different nuclear forces and energy considerations. The nucleus initially has a prolate shape in the ground state, which is energetically favorable due to the arrangement of nucleons and the dominant nuclear forces acting within the nucleus. However, when the excitation energy increases, quantum shell effects emerge, and nucleons rearrange themselves. This rearrangement can favor a different deformation, which causes the nucleus to shift from its prolate ground state to an oblate configuration.

Let's focus specifically on the ^{122}Ru nucleus that shows different deformation behavior. As shown in Figs 2 and 3, the PES of ^{122}Ru is almost spherical, and the rising hill is pushing it towards the right, making it more axial (prolate). According to the analysis of the PES, assuming triaxial deformation Fig. 2, ^{152}Ba isotopes display prolate deformation at their absolute minima. In the axial deformation Fig. 3, the prolate solution is more profound than the oblate one. Consequently, for this particular nucleus, it is clear that the prolate solution is the absolute minimum. As the neutron number increases, the energy of the oblate solution decreases, and it approaches the energy of the prolate solution. The same behavior appears in the ^{166}Sm nucleus, increasing the depth of both prolate oblate and the development of a pronounced prolate deformation, much more rigid regarding the γ degree of freedom. Similar behavior is predicted in ^{186}Er nucleus, where the shape coexistence appears also. The local energy minimum is located at (β, γ) = (0.32, 5º) in the prolate deformed region, which is obviously higher than the prolate deformed minimum. In the case when axial symmetry is assumed Fig. 3, rapid transitions appeared between strongly prolate deformed minima to oblate minimum, in clear indication of the shape coexistence, which matches the behavior in the triaxial deformation.

In the following section, we will focus on the nuclei that exhibit significant nuclear deformation, which is noticeable from the previous Figures. For this purpose, the distribution of protons, neutrons, neutron kinetic densities, and neutron pairing potential in terms of energy will be analyzed. Fig. 4 shows the axial neutron and proton density corresponding to a local minimum on the PEC for a ^{100}Kr nucleus using the HF + BCS method. The oblate deformation is clearly seen, where the contours of proton and neutron densities reveal unsymmetric patterns, indicating an unequal distribution of neutrons and protons, emphasizing the existence of nuclear deformations. Furthermore, the central region in the neutron density suggests high density where neutrons are tightly packed together, forming a dense core. In contrast, proton density contours in the same region indicate slightly lower density than neutron ones. This pattern stems from the significant difference between the number of neutrons and protons, which is reflected in the distribution of nucleons within the nucleus and its shapes. Although the neutron density is high in the central nucleus region, we cannot necessarily assume that the neutron's kinetic density will be equally high. The relationship between the mass density and kinetic density of neutrons is not always directly proportional. Various factors, such as the nuclear structure and interactions between nucleons, influence the kinetic energy distribution of neutrons in a nucleus. These factors can lead to fluctuations in the density of neutron kinetic energy even in areas with high neutron mass density. Generally, pairing energy is more vital in nuclei with even protons and neutrons than in nuclei with an odd number of protons or neutrons, known as the pairing effect. Based on the neutron pairing potential, it is obvious that in the central region, the neutron pairing potential is relatively weak. This could demonstrate that neutron pairs in this region undergo weaker attractive interaction compared to other regions in the nucleus. The red-colored arc-shaped regions indicate a higher neutron pairing potential. This suggests that neutron pairs experience a stronger attractive interaction in this area, resulting in lower energy states for these paired neutrons. These regions are surrounded by a yellow color, which could indicate a distinct region in the nucleus where the neutron pairing potential behaves differently than its surroundings. The contrast with the surrounding yellow color suggests that the neutron pairing potential in this region is significantly higher.

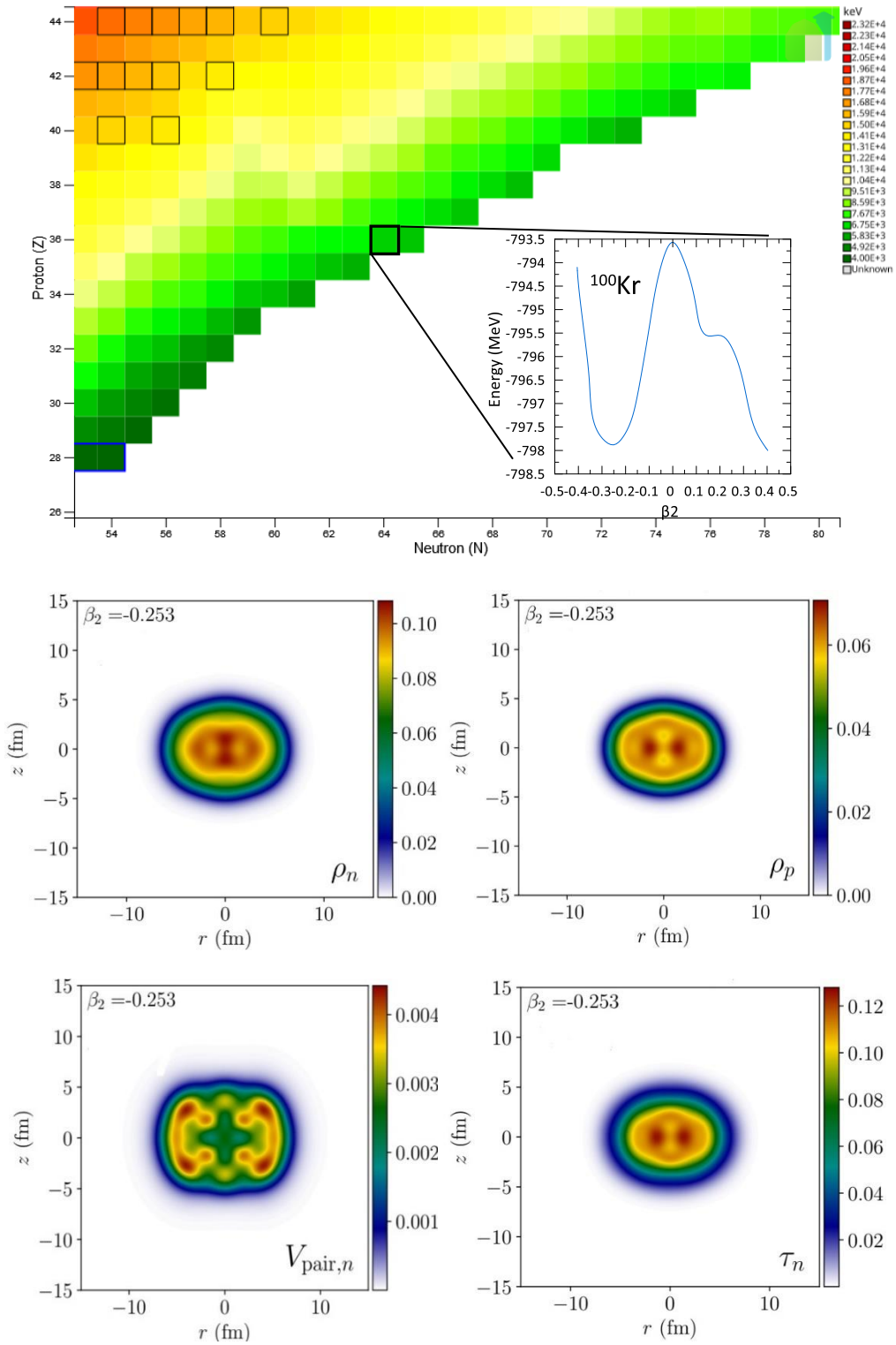

Fig. 4. The neutron, proton, neutron pairing, and neutron kinetic energy for β_2 minima in ^{100}Kr nucleus. (See color Figure on the journal website.)

For ^{152}Ba, Fig. 5, the axial neutron density contour plot typically displays a prolate shape with the highest density at the center of the nucleus, gradually decreasing towards the edges. In the central region, the proton density plot differs slightly from the neutron one due to the influence of the nucleus's electromagnetic forces. The most exciting feature can be noticed in the neutron pairing potential. The neutron pairing potential displays a unique characteristic. It promotes the existence of an even number of neutrons, resulting in nuclear structures with an even number of neutrons being more stable than those with an odd number. The colors of the couture plot help us more imaginatively grasp the relative behavior of the neutron pairing

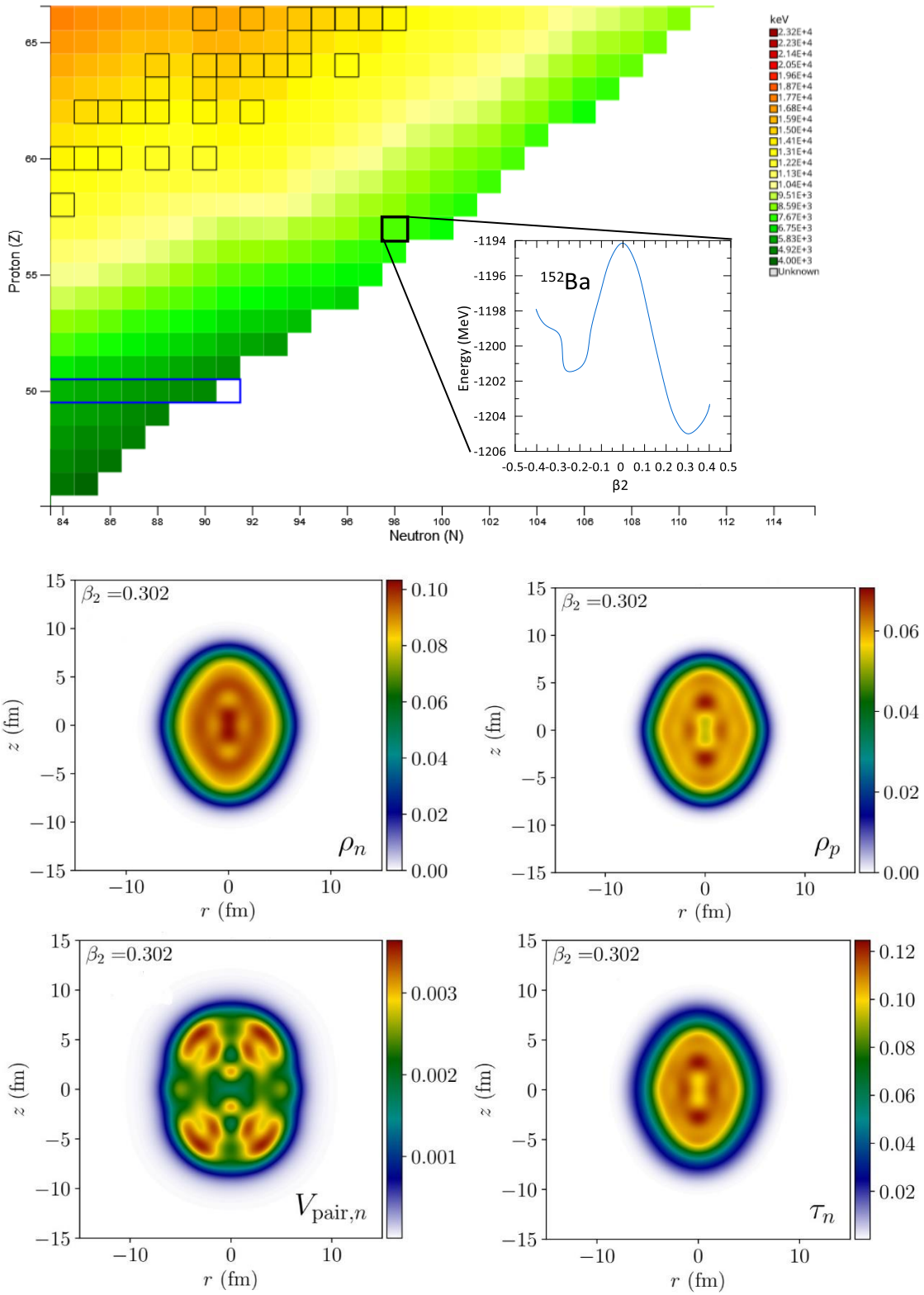

Fig. 5. The neutron, proton, neutron pairing, and neutron kinetic energy for β_2 minima in ^{152}Ba nucleus. (See color Figure on the journal website.)

potential. The broadening prolate shape, with four red regions at the upper and lower corners, surrounded by yellow and green regions, paints a vivid picture of the neutron pairing potential. The presence of red regions at the upper and lower corners indicates areas of high neutron pairing energy. This suggests strong pairing interactions occur in those regions, resulting in greater stability and coherence of neutron pairs. The surrounding yellow and green regions, on the other hand, represent areas with lower pairing energy. These regions may indicate weaker pairing interactions, where the neutron pairs are less stable or tightly bound.

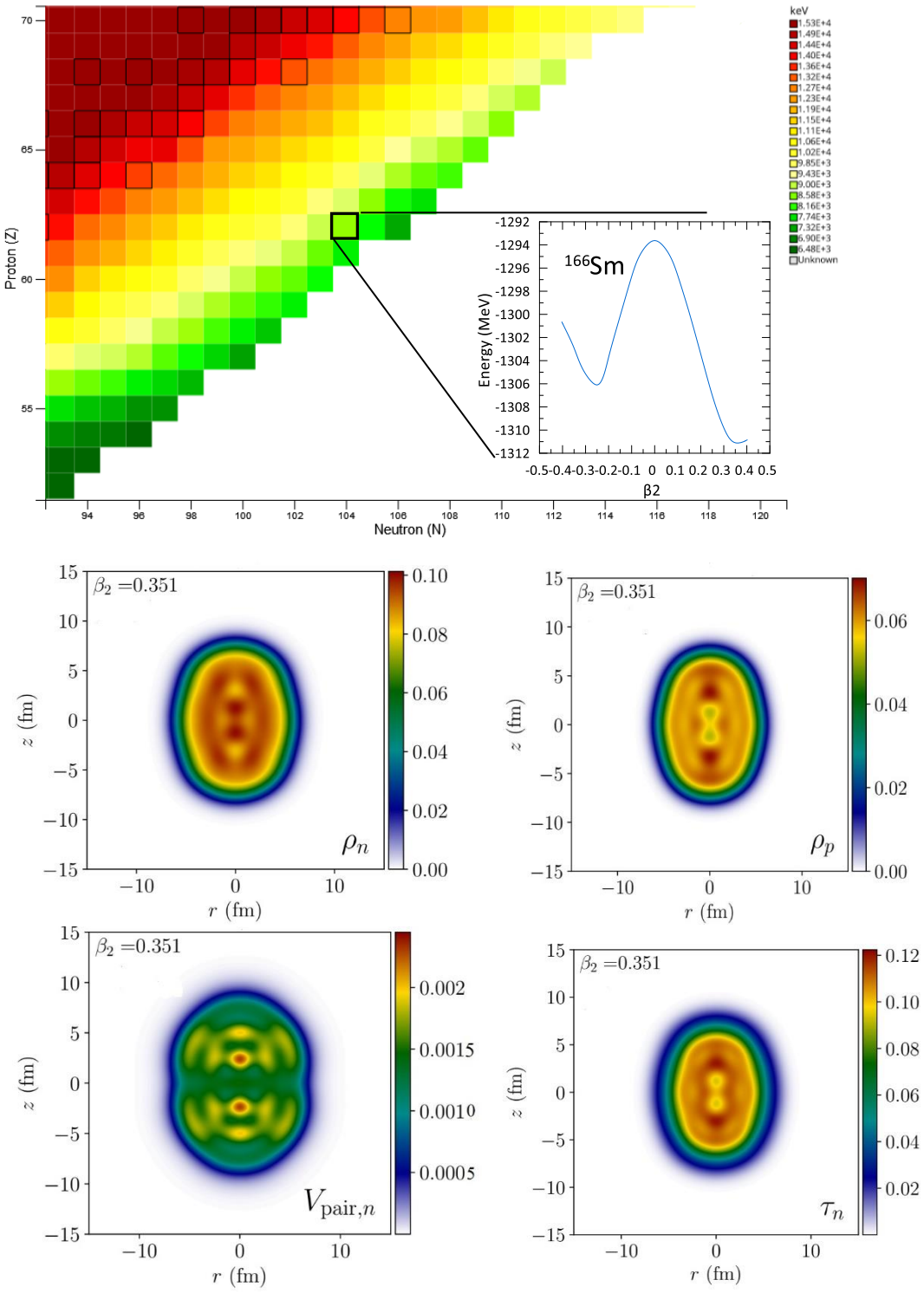

Fig. 6. The neutron, proton, neutron pairing, and neutron kinetic energy for β_2 minima in ^{166}Sm nucleus. (See color Figure on the journal website.)

In Fig. 6, we illustrate the variation of axial neutron and proton density corresponding to a prolate local minimum on the PEC for ^{166}Sm nucleus. In the neutron density plot, we can observe two small vertical red spots in the central area, indicating a higher concentration of neutrons. This could be due to a localized concentration of neutrons in this region. The concentration of neutrons decreases gradually, forming a transitional zone. Moving outward from the red spots, we encounter thin orange-yellow prolate regions indicating a moderate neutron density. These regions represent areas where the neutron concentration is slightly lower than the central red spots but still higher than the cyan and blue regions. The concentration of neutrons gradually decreases, forming a transitional zone. The density contrast between neutrons

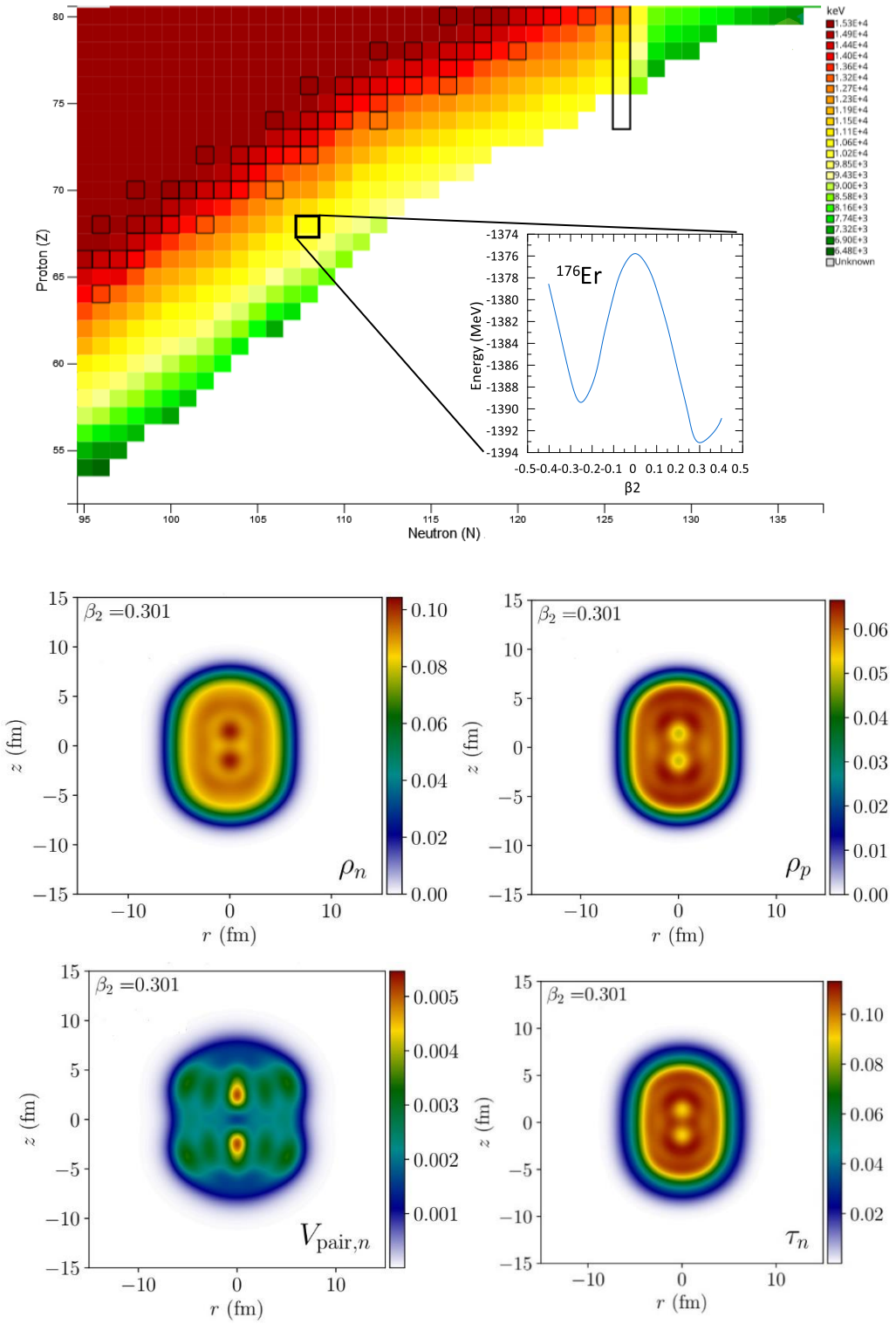

Fig. 7. The neutron, proton, neutron pairing, and neutron kinetic energy for β_2 minima in ^{176}Er nucleus. (See color Figure on the journal website.)

and protons is most strikingly evident in the nucleus's central region. As previously explained, the neutron's density reflects its mass distribution within a given space. Meanwhile, the kinetic density of a neutron reveals how its kinetic energy is distributed within that space. These two measures are separate and can show varying patterns within the nucleus. The most essential and noteworthy behavior in selected neutron-rich nuclei is neutron pairing potential, which can be tracked by comparing the evolution of its shapes. The imbalance in the number of protons and neutrons in neutron-rich heavy nuclei can cause an odd imbalance. This imbalance can affect the pairing energy, as the pairing force decreases with increasing numbers of neutrons. When extra neutrons are in the nucleus, they can combine, further reducing the ove-

rall pairing energy. Furthermore, increasing the number of protons in neutron-rich heavy nuclei can disrupt the pairing of nucleons due to the stronger Coulomb repulsion between the protons.

This behavior is also confirmed in Fig. 7 of ^{176}Er nucleus, where the regions of high energies gradually decrease to lower ones. Also, it can be noticed that the broadening prolate shapes clearly appeared in the neutron and proton densities, which are primarily due to the interplay of nuclear potential and the pairing correlations. The pairing interaction causes nucleons to align along the nucleus's long axis, producing a prolate shape. This alignment is due to the interplay between the pairing interaction and the mean-field potential.

5. Conclusions

In conclusion, the results of this study provide valuable information and shed light on the triaxial and axial deformation of the neutron-rich heavy nuclei near the drip line. Through rigorous data analysis, we have uncovered insightful patterns and correlations contributing to our understanding of pairing potential energy and deformation in such heavy nuclei, which have significant implications and pave the way for future research. The magic numbers suggest that nuclei have a spherical shape. However, in the case of the ^{24}Si nucleus (with Z = 14 and N = 28), there is a coexistence of shapes due to the interaction between shell structure, particle interactions, and nuclear forces. The shape of the nucleus is still affected by the nucleons' collective behavior and energy levels. For neutron-rich heavy nuclei near the dripline, their shapes smoothly transition from spherical to triaxial and then prolate around β_2 values ranging from 0.2 to 0.4. The SHF + BCS mean-field method was used for axial deformation analysis, which confirmed our RHB method results for triaxial deformation analysis. An imbalance in protons and neutrons can affect pairing energy, where the extra neutrons can reduce overall pairing energy, and the protons can disrupt nucleon pairing due to stronger Coulomb repulsion between protons.

REFERENCES

1. K. Heyde. *Basic Ideas and Concepts in Nuclear Physics.* 2nd edition (Bristol and Philadelphia: Institute of Physics Publishing, 1999) 524 p.
2. N. Takigawa, K. Washiyama. *Fundamentals of Nuclear Physics* (Tokyo-Japan: Springer, 2017) 269 p.
3. A. Shukla, S. K. Patra (Eds.). *Nuclear Structure Physics* (Taylor & Francis Group, 2020) 416 p.
4. W. Koepf, P. Ring. Has the nucleus ^{24}Mg a triaxial shape? a relativistic investigation. Phys. Lett. B 212 (1988) 397.
5. G.A. Lalazissis, M.M. Sharma. Ground-state properties of exotic nuclei near Z = 40 in the relativistic mean-field theory. Nucl. Phys. A 586 (1995) 201.
6. D. Hirata et al. Triaxial deformation of unstable nuclei in the relativistic mean-field theory. Nucl. Phys. A 609 (1996) 131.
7. J.M. Yao et al. Candidate multiple chiral doublets nucleus ^{106}Rh in a triaxial relativistic mean-field approach with time-odd fields. Phys. Rev. C 79 (2009) 067302.
8. Z.P. Li et al. Relativistic energy density functionals: Low-energy collective states of ^{240}Pu and ^{166}Er. Phys. Rev. C 81 (2010) 064321.
9. J.M. Yao. Configuration mixing of angular-momentum-projected triaxial relativistic mean-field wave functions. II. Microscopic analysis of low-lying states in magnesium isotopes. Phys. Rev. C 83 (2011) 014308.
10. B.-N. Lu et al. Multidimensionally-constrained relativistic mean-field models and potential-energy surfaces of actinide nuclei. Phys. Rev. C 89 (2014) 014323.
11. W.X. Xue et al. Triaxially deformed relativistic point-coupling model for Λ hypernuclei: A quantitative analysis of the hyperon impurity effect on nuclear collective properties. Phys. Rev. C 91 (2015) 024327.
12. H. Abusara, S. Ahmad. Shape evolution in Kr, Zr, and Sr isotopic chains in covariant density functional theory. Phys. Rev. C 96 (2017) 064303.
13. J.-U. Nabi et al. The nuclear ground-state properties and stellar electron emission rates of ^{76}Fe, ^{78}Ni, ^{80}Zn, ^{126}Ru, ^{128}Pd and ^{130}Cd using RMF and pn-QRPA models. Nucl. Phys. A 1015 (2021) 122278.
14. V. Kumar et al. The microscopic studies of the even-even $^{12-28}$O, $^{34-60}$Ca, $^{48-80}$Ni, and $^{100-134}$Sn using covariant density functional theory. Nucl. Phys. A 1022 (2022) 122429.
15. Y.-T. Rong et al. Anatomy of octupole correlations in ^{96}Zr with a symmetry-restored multidimensionally-constrained covariant density functional theory. Phys. Lett. B 840 (2023) 137896.
16. T. Nikšić et al. DIRHB – A relativistic self-consistent mean-field framework for atomic nuclei. Comput. Phys. Commun. 185(6) (2014) 1808.
17. H.A. Bahr, A.A. Alzubadi. Relativistic and nonrelativistic mean field analysis of the shell evolution in $^{44-52}$Ar isotopes. Int. J. Mod. Phys. E 31(4) (2022) 2250029.
18. A.A. Allami, A.A. Alzubadi. Study of the nuclear structure of some exotic nuclei using nonrelativistic and relativistic mean-field methods. Int. J. Mod. Phys. E 29(12) (2020) 2050090.
19. W. Koepf, P. Ring. A relativistic description of rotating nuclei: The yrast line of ^{20}Ne. Nucl. Phys. A 493(1) (1989) 61.
20. P. Ring, P. Schuck. *The Nuclear Many-Body Problem* (Berlin: Springer-Verlag, 1980).
21. A. Staszczak et al. Augmented Lagrangian method

for constrained nuclear density functional theory. Eur. Phys. J. A 46 (2010) 85.
22. A. Bohr, B.R. Mottelson. *Nuclear Structure*. In 2 volumes (New York, USA: Benjamin, 1975) 1256 p.
23. A.A. Alzubadi. Investigation of nuclear structure of $^{30\text{-}44}$S isotopes using spherical and deformed Skyrme-Hartree-Fock method. Indian J. Phys. 89 (2015) 619.
24. A.A. Alzubadi, R.S. Obaid. An analysis of the tensor force and pairing correlation on the disappearance of nuclear magicity at N = 28 region. Braz. J. Phys. 53 (2023) 99.
25. J.-P. Delaroche et al. Structure of even-even nuclei using a mapped collective Hamiltonian and the D1S Gogny interaction. Phys. Rev. C 81 (2010) 014303.
26. P. Möller et al. Nuclear ground-state masses and deformations: FRDM (2012). At. Data Nucl. Data Tables 109-110 (2016) 1.
27. A. Gade, S.N. Liddick. Shape coexistence in neutron-rich nuclei. J. Phys. G 43 (2016) 024001.

А. А. Алзубаді*, С. М. Алдулаімі

Фізичний факультет, Науковий коледж, Багдадський університет, Багдад, Ірак

*Відповідальний автор: ali.abdullatif@sc.uobaghdad.edu.iq

ТРИАКСІАЛЬНА ДЕФОРМАЦІЯ ЯДЕР ПОБЛИЗУ ЛІНІЇ НЕЙТРОННОЇ НЕСТАБІЛЬНОСТІ ЗА ДОПОМОГОЮ АНАЛІЗУ РЕЛЯТИВІСТСЬКОГО СЕРЕДНЬОГО ПОЛЯ

Дане дослідження присвячено деформації нейтронно-збагачених ядер поблизу лінії нейтронної нестабільності. Розглянуті ядра включають ^{28}O, ^{42}Si, ^{58}Ca, ^{80}Ni, ^{100}Kr, ^{122}Ru, ^{152}Ba, ^{166}Sm і ^{176}Er. Для дослідження триаксіальної деформації використовується релятивістський метод Хартрі - Боголюбова (RHB) з ефективним точковим зв'язком, що залежить від густини, а для аналізу аксіальної деформації використовується метод Скірма - Хартрі - Фока + Бардіна - Купера - Шріффера. Дослідження мало на меті зрозуміти зв'язок між ядерними силами, взаємодією частинок і оболонковою структурою, щоб отримати уяву про унікальну поведінку багатих нейтронами ядер. Незважаючи на те, що ці ядра містять магічні числа, на їхню форму все ще впливає колективна поведінка нуклонів та рівні енергії. Зі збільшенням кількості нейтронів форма плавно переходить від сферичної до триаксіальної, а потім до витягнутої. Аналіз аксіальної деформації підтвердив результати аналізу триаксіальної деформації методом RHB. Дисбаланс у кількості протонів і нейтронів може вплинути на енергію спарювання, де додаткові нейтрони можуть зменшити загальну енергію спарювання, а протони можуть порушити спарювання нуклонів через сильніше кулонівське відштовхування між ними.

Ключові слова: релятивістське середнє поле, Хартрі - Фок + Бардін - Купер - Шріффер, тривісна деформація, нейтронна крапельниця, колективний рух.

Надійшла / Received 05.04.2024